

ENGINEERING APPROACH TO MODELLING FREQUENCY DISPERSION WITHIN NORMAL METALS AT ROOM TEMPERATURE FOR THz APPLICATIONS

S. Lucyszyn and Y. Zhou

Optical and Semiconductor Devices Group
Department of EEE
Imperial College London
SW7 2AZ, London, United Kingdom

Abstract—When compared to the over-simplified classical skin-effect model, the accurate classical relaxation-effect modelling approach for THz structures at room temperature can be mathematically cumbersome and not insightful. This paper introduces various interrelated electrical engineering concepts as tools for characterizing the intrinsic frequency dispersive nature of normal metals at room temperature. This engineering approach dramatically simplifies the otherwise complex analysis and allows for a much deeper insight to be gained into the classical relaxation-effect model. For example, it explains how wavelength can increase proportionally with frequency at higher terahertz frequencies. This is the first time that such an approach has been developed for the modelling of intrinsic frequency dispersion within a metal. While the focus has been on the characterization of normal metals (magnetic and non-magnetic) at room temperature, it is believed that the same methodology may be applied to metals operating in anomalous frequency-temperature regions, superconductors, semiconductors, carbon nanotubes and metamaterials.

1. INTRODUCTION

The accurate characterization of frequency dispersion within normal metals at room temperature was first introduced over a century ago, by Drude [1,2], and its robustness has been tested in recent years for normal metals at room temperature from dc to terahertz frequencies [3–7]. For example, it has been used to validate

Corresponding author: S. Lucyszyn (s.lucyszyn@imperial.ac.uk).

measurements [3], alternative frequency dispersion models [4, 5] and commercial electromagnetic simulation software [6]. However, when compared to the over-simplified classical skin-effect model, the accurate classical relaxation-effect modelling approach for THz structures at room temperature can be mathematically cumbersome and not insightful. This paper introduces various interrelated electrical engineering concepts as tools for characterizing intrinsic frequency dispersion models.

Given an angular frequency $\omega = 2\pi f$, where f is the frequency of the driving electromagnetic fields, and the phenomenological temperature-dependent scattering relaxation time for the free electrons (i.e., mean time between collisions) τ , with normal metals at room temperature, a microwave engineer more often adopts the classical skin-effect model, where $\omega\tau \ll 1$, without quantifying the resulting errors at terahertz frequencies. Conversely, the physicist may adopt the accurate classical relaxation-effect model, but then make simplifying assumptions (e.g., $\omega\tau \ll 1$ or $\omega\tau \gg 1$), again without quantifying the resulting errors at terahertz frequencies. For normal metals that avoid anomalous frequency-temperature regions of behaviour, this paper addresses all values of $\omega\tau$ and even allows accurate simplifying assumptions to be made in the region from dc to $\omega\tau = 2$.

2. EQUIVALENT TRANSMISSION LINE MODELLING

The analogy between the characteristics of electromagnetic waves as they propagate within a homogenous material and down a transmission line can be seen by comparing the vector Helmholtz equations (for an unbounded plane wave as it travels in one-dimensional space) with those of the telegrapher's equations.

With the former, for a uniform electromagnetic plane wave travelling at normal incidence to the surface of a semi-infinite half space, the intrinsic impedance η_I of a homogeneous material and the corresponding propagation constant have the general forms given by:

$$\eta_I = \sqrt{\frac{j\omega\mu}{\sigma + j\omega\varepsilon}} = \sqrt{\frac{(\omega\mu_o\mu_r'') + j\omega(\mu_o\mu_r')}{(\sigma' + \omega\varepsilon_o\varepsilon_r'') + j\omega\left(\frac{-\sigma''}{\omega} + \varepsilon_o\varepsilon_r'\right)}} \quad [\Omega] \quad (1)$$

$$\begin{aligned} \gamma &\equiv \frac{j\omega\mu}{\eta_I} = \sqrt{j\omega\mu(\sigma + j\omega\varepsilon)} \\ &= \sqrt{[(\omega\mu_o\mu_r'') + j\omega(\mu_o\mu_r')] \left[(\sigma' + \omega\varepsilon_o\varepsilon_r'') + j\omega\left(\frac{-\sigma''}{\omega} + \varepsilon_o\varepsilon_r'\right) \right]} \quad [\text{m}^{-1}] \quad (2) \end{aligned}$$

where the relative magnetic permeability $\mu_r = \mu/\mu_o \equiv \mu_r' - j\mu_r''$, μ_o is

the magnetic permeability of free space; relative electric permittivity due to molecular and atomic resonances, $\epsilon_r = \epsilon/\epsilon_o \equiv \epsilon'_r - j\epsilon''_r$, ϵ_o is the electric permittivity of free space; and intrinsic bulk conductivity due to free charge carriers, $\sigma \equiv \sigma' - j\sigma''$. With the latter, the characteristic impedance Z_o and propagation constant γ for a uniform transmission line with infinite length have the general forms given by:

$$Z_o = \sqrt{\frac{R + j\omega L}{G + j\omega C}} \quad [\Omega] \tag{3}$$

$$\gamma \equiv \frac{R + j\omega L}{Z_o} = \sqrt{(R + j\omega L)(G + j\omega C)} \quad [\text{m}^{-1}] \tag{4}$$

The direct mathematical relationship between the constitutive terms in (1) and (2) and distributed-element parameters in (3) and (4) is well known, for example given by Kraus [8]. As a result, electromagnetic wave propagation within a homogeneous material can be represented by the textbook equivalent one-dimensional uniform transmission line (or distributed-element) model shown in Fig. 1, terminated by the secondary line parameter characteristic impedance Z_o .

The equivalent primary line (i.e., distributed-element) parameters for this generic case are given by the following:

$$R \equiv \omega\mu_o\mu''_r \quad [\Omega/\text{m}]; \quad L \equiv \mu_o\mu'_r \quad [\text{H}/\text{m}];$$

$$G \equiv \sigma' + \omega\epsilon_o\epsilon''_r \quad [\text{S}/\text{m}]; \quad C \equiv \frac{-\sigma''}{\omega} + \epsilon_o\epsilon'_r \quad [\text{F}/\text{m}]$$

It will now be shown that be-spoke elementary lumped-element circuits can be synthesized to represent various intrinsic frequency dispersion models for a normal metal at room temperature. For the elementary lumped-element circuits to be valid, the distance of propagation Δz must be very much shorter than the wavelength λ of the electromagnetic wave within the metal. The resulting transmission

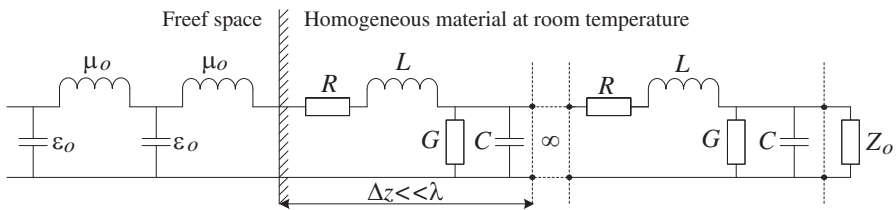


Figure 1. Generic equivalent transmission line model for a homogeneous material at room temperature showing distributed-element parameters.

line model analogy is useful for giving a pedagogical insight into the behaviour of the electromagnetic waves as they try to propagate into a normal metal at room temperature. In addition, it can be used as a general predictive model for characterizing both the reflection and transmission characteristics of the metal.

2.1. Classical Skin-effect Modelling

With the over-simplified classical skin-effect model, familiar to microwave engineers, electron scattering relaxation and displacement current terms are ignored (i.e., $\omega\tau \cong 0$ and $\omega\varepsilon_o \cong 0$, respectively) and for normal metals at room temperature the constitutive parameters are represented by the following: $\mu \rightarrow \mu_o$; $\varepsilon \rightarrow \varepsilon_o \cong 0$; $\sigma \rightarrow \sigma_o$, where σ_o is the bulk conductivity at dc. As a result, the characteristic impedance Z_{o_o} is now given by the well-known textbook expression for the classical skin-effect model surface impedance Z_{S_o} (associated variables for this model are indicated by the suffix “o”):

$$Z_{o_o} = \sqrt{\frac{R_o + j\omega L_o}{G_o + j\omega C_o}}$$

and $\gamma_o \equiv \frac{R_o + j\omega L_o}{Z_{o_o}} = \sqrt{(R_o + j\omega L_o)(G_o + j\omega C_o)}$ (5)

$$Z_{o_o} \Rightarrow \eta_{I_o} = \sqrt{\frac{j\omega\mu_o}{\sigma_o}} \Rightarrow Z_{S_o} \equiv (R_{S_o} + jX_{S_o}) \quad [\Omega/\text{square}]$$

where $X_{S_o} \equiv R_{S_o}$; $R_{S_o} \equiv \Re\{Z_{S_o}\} = \sqrt{\frac{\omega\mu_o}{2\sigma_o}}$ [Ω/square]; $L_{S_o} \equiv \frac{\Im\{Z_{S_o}\}}{\omega} = \sqrt{\frac{\mu_o}{2\omega\sigma_o}}$ [H/square].

Therefore, the distributed-element parameters for the classical skin-effect model become:

$$R_o = 0; \quad L_o = \mu_o; \quad G_o = \sigma_o; \quad C_o = \varepsilon_o \cong 0$$

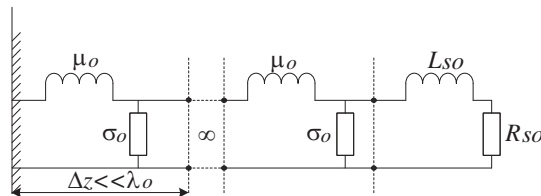


Figure 2. Equivalent transmission line model for the classical skin-effect model.

The equivalent one-dimensional uniform transmission line model of Fig. 1 simplifies to that shown in Fig. 2. It is interesting to note that these parameters are frequency invariant, but with $\sigma_o \propto \tau$ there is a strong temperature dependence.

2.2. Classical Relaxation-effect Modelling

With the accurate classical relaxation-effect model, more familiar with physicists, displacement current can still be ignored at terahertz frequencies but scattering relaxation cannot be and so the constitutive parameters are represent by the following: $\mu \rightarrow \mu_o$; $\varepsilon \rightarrow \varepsilon_o \cong 0$; $\sigma \rightarrow \sigma_R = \frac{\sigma_o}{1+j\omega\tau}$. The intrinsic frequency behavior of the bulk conductivity has exactly the same form as the transfer function of a first-order Butterworth (maximally-flat) R - C low-pass filter (having a monotonically changing magnitude frequency characteristic with -20 dB per decade roll off response, beyond its -3 dB cut-off frequency at $f_\tau = 1/(2\pi\tau)$, where the time constant for this filter is $\tau = RC$). The characteristic impedance Z_{oR} is now given by the classical relaxation-effect model surface impedance Z_{SR} (associated variables for this model are indicated by the suffix “ R ”):

$$Z_{oR} = \sqrt{\frac{R_R + j\omega L_R}{G_R + j\omega C_R}}$$

and $\gamma_R \equiv \frac{R_R + j\omega L_R}{Z_{oR}} = \sqrt{(R_R + j\omega L_R)(G_R + j\omega C_R)}$ (6)

$$Z_{oR} \Rightarrow \eta_{IR} \cong \sqrt{\frac{j\omega\mu_o}{\left[\frac{\sigma_o}{1+(\omega\tau)^2}\right] + j\omega\left[\frac{-\tau\sigma_o}{1+(\omega\tau)^2}\right]}} \Rightarrow Z_{SR} \equiv (R_{SR} + jX_{SR})$$

where $R_{SR} \equiv \Re\{Z_{SR}\} = \frac{R_{So}}{(1+\xi\omega\tau)}$; $L_{SR} \equiv \Im\{Z_{SR}\} = \frac{R_{So}}{\omega}(1 + \xi\omega\tau)$.

$$\xi = \sqrt{\sqrt{u^{-4} + u^{-2}} + u^{-1} - u^{-1}} \quad \text{and} \quad u = (\omega\tau) \quad (7)$$

Note that the uniquely-defined variable ξ in (7) can greatly simplify analytical expressions. From (6), the distributed-element parameters for the classical relaxation-effect model become:

$$R_R = 0; \quad L_R = \mu_o; \quad G_R = \frac{\sigma_o}{1 + (\omega\tau)^2};$$

$$C_R = \frac{-\tau\sigma_o}{1 + (\omega\tau)^2} + \varepsilon_o \cong \frac{-\tau\sigma_o}{1 + (\omega\tau)^2}$$

The resulting equivalent one-dimensional uniform transmission line model of Fig. 1 can now be represented by the new model shown in

Fig. 3(a). It is interesting to note that there is now a strong dependence with both temperature and frequency for the shunt elements and the complete distributed-element model. As an alternative solution, the elementary lumped-element circuit in Fig. 3(a) can be reconfigured, such that the negative distributive shunt capacitance is transformed into an equivalent positive distributive shunt inductance:

$$L_{SHUNT_R} \equiv \frac{-1}{\omega^2 C_R \Delta z^2} = \frac{1 + (\omega\tau)^2}{\omega^2 \tau \sigma_o \Delta z^2} \quad [\text{H/m}] \quad (8)$$

The resulting alternative distributed-element model is shown in Fig. 3(b). By inspection, it can be seen that Fig. 3(b) represents a more realistic model, as the negative shunt capacitance in Fig. 3(a) is avoided.

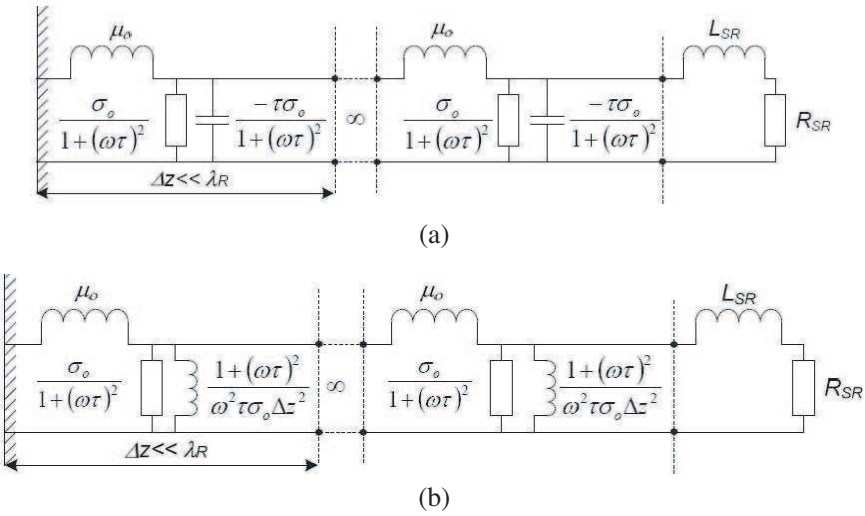


Figure 3. Equivalent transmission line models for the classical relaxation-effect model.

Table 1. Circuit-based simulation results for gold at room temperature (with $\omega\tau = 1$, depth $l = \lambda_R$, $\Delta z = \lambda_R/400 = 1.067$ [nm]).

Equivalent Transmission Line model	Elementary Lumped-element Circuit Values					Z_{IN} [Ω]	τ_{pR} [fs/ λ_R] from (9)
	$R_R \cdot \Delta z$ [Ω]	$L_R \cdot \Delta z$ [fH]	$G_R \cdot \Delta z$ [mS]	$C_R \cdot \Delta z$ [fF]	$L_{SHUNT_R} \cdot \Delta z$ [pH]	$Z_T = Z_{SR}$	
Fig. 3(a)	—	1.341	24.1	-0.654	—	$0.4607 + j1.137$	170.491
Fig. 3(b)	—	1.341	24.1	—	1.126	$0.4607 + j1.137$	170.491

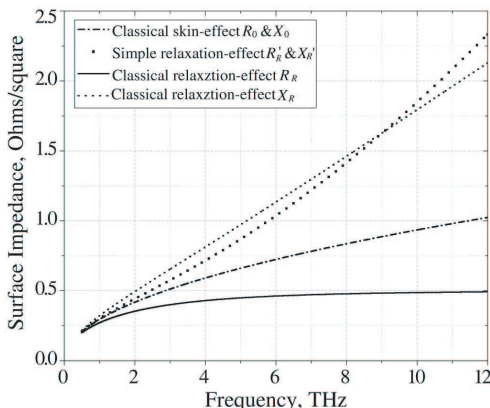


Figure 4. Calculated values of surface impedance for gold at room temperature.

The surface impedance for gold at room temperature (having $\sigma_o = 4.517 * 10^7$ [S/m], $\tau = 27.135$ [fs], $\mu_r = 0.99996 \cong 1$ [3]) is shown in Fig. 4, for different intrinsic frequency dispersion models. When compared to the classical skin-effect model, with reference to Fig. 2, it can be deduced that the introduction of the shunt inductance accounts for the higher values of surface inductive reactance [6]. Moreover, using network analysis, it can be shown that the shunt inductance also accounts for the lower values of surface resistance [6]. Here, the shunt inductive reactance effectively couples more energy into the following section and, therefore, less energy is dissipated in the preceding section.

It is important to note that while many variations of the generic equivalent transmission line model in Fig. 1 can be synthesized, either by combining (1) with (3) or (2) with (4), they are only limited to predicting either the surface impedance or propagation constant, respectively. In contrast, Fig. 3 represents two models that have been synthesized using both the combination of (1) with (3) and (2) with (4), and can therefore be used as a general predictive model for characterizing both reflection and transmission characteristics.

For example, with gold at room temperature, at $\omega\tau = 1$ and with a depth $l = \lambda_R$, it can be shown through general material calculations that $Z_{SR} = \sqrt{j\omega\mu/\sigma_R} = 0.4608 + j1.1124$ [Ω/square], $\gamma_R = j\omega\mu/Z_{SR} = \sqrt{j\omega\mu\sigma_R} = 35.532 + j14.719$ [μm^{-1}], $\lambda_R = 2\pi/\Im\{\gamma_R\} = 426.898$ [nm] and transit time propagation delay $\tau_{pR} = \Im\{\gamma_R\} \cdot l/\omega \rightarrow 1/f_\tau = 2\pi\tau = 170.494$ [fs/ λ_R]. Using commercial circuit simulation software (AWR's Microwave Office[®]), as expected, the reflection characteristic of input impedance Z_{IN} for 400 cascaded elementary lumped-element circuit

sections, terminated at the far end with an impedance $Z_T = Z_{SR}$, is equal to Z_{SR} . Also, the corresponding transmission characteristic of propagation delay per unit wavelength can be calculated from the following circuit-based equations.

$$\begin{aligned} \tau_{pR} &= \frac{l}{v_{pR}} \rightarrow \frac{\lambda_R}{v_{pR}} = \frac{1}{f} [s/\lambda_R] \\ \text{where } \lambda_R &= \frac{2\pi}{\Im\{\gamma_R|_{\text{Fig. 3}}\}}; \quad v_{pR} = \frac{\omega}{\Im\{\gamma_R|_{\text{Fig. 3}}\}} \\ \gamma_R|_{\text{Fig. 3}} &= \sqrt{j\omega L_R(G_R + j\omega C_R)} \\ &= \sqrt{j\omega L_R \left(G_R - j \frac{1}{\omega L_{SHUNT_R} \Delta z^2} \right)} \equiv \sqrt{j\omega \mu \sigma_R} \end{aligned} \quad (9)$$

The results from this circuit-based approach are given in Table 1 and these can be compared with the previous materials-based calculations. It can be seen that there is excellent agreement, which further improves as $\lambda_R/\Delta z$ increases.

2.3. Simple Relaxation-effect Modelling

Because of limitations found with some electromagnetic simulation software (i.e., not being able to utilize the imaginary part of bulk conductivity), the results from the simple relaxation-effect model are generated instead of those from the intended classical relaxation-effect model [6]. With this erroneous simple relaxation-effect model, the constitutive parameters can be represent by the following: $\mu \rightarrow \mu_o$; $\varepsilon \rightarrow \varepsilon_o \cong 0$; $\sigma \rightarrow \sigma_{R'} = \frac{\sigma_o}{1+(\omega\tau)^2}$. As a result, the characteristic impedance is now given by the simple relaxation-effect model surface impedance $Z_{SR'}$ (associated variables for this model are indicated by the suffix "R'"):

$$\begin{aligned} Z_{OR'} &= \sqrt{\frac{R_{R'} + j\omega L_{R'}}{G_{R'} + j\omega C_{R'}}} \\ \text{and } \gamma_{R'} &\equiv \frac{R_{R'} + j\omega L_{R'}}{Z_{OR'}} = \sqrt{(R_{R'} + j\omega L_{R'}) (G_{R'} + j\omega C_{R'})} \\ Z_{OR'} &\Rightarrow \eta_{IR'} \cong \sqrt{\frac{j\omega \mu_o}{\sigma_{R'}}} = \sqrt{\frac{j\omega \mu_o}{\left[\frac{\sigma_o}{1+(\omega\tau)^2} \right]}} \Rightarrow Z_{SR'} \equiv (R_{SR'} + jX_{SR'}) \end{aligned} \quad (10)$$

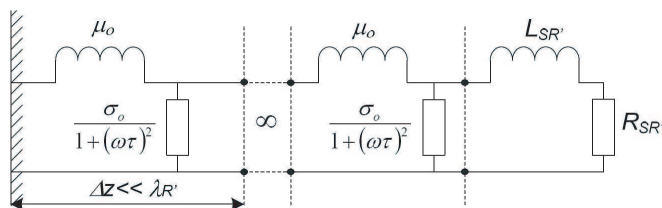


Figure 5. Equivalent transmission line model for the simple relaxation-effect model.

Therefore, from (10), the distributed-element parameters for the simple relaxation-effect model become:

$$R_{R'} = 0; \quad L_{R'} = \mu_0; \quad G_{R'} = \frac{\sigma_0}{1 + (\omega\tau)^2}; \quad C_{R'} = 0$$

The resulting equivalent one-dimensional uniform transmission line model of Fig. 1 is represented by the model shown in Fig. 5. Once again, there is a strong dependence with both temperature and frequency for the shunt element and the complete distributed-element model.

When compared to the classical skin-effect model, with reference to Fig. 2, it can be seen that the simple relaxation-effect model is similar, but the shunt conductance is lower and now also frequency dependent. Obviously, the lower shunt conductance will account for the higher surface resistance found in Fig. 4 [6]. Moreover, using network analysis, it can be shown that the lower values of shunt conductance in Fig. 5 will increase coupling into the following section. As a result, more inductance will be seen by the preceding stage and this accounts for the higher surface inductive reactance found in Fig. 4 [6].

When compared with the classical relaxation-effect model, it can be seen that the simple relaxation-effect model is similar, but with the shunt inductance removed from the elementary lumped-element circuit. Since the simple relaxation-effect model is inherently erroneous it will not be considered further.

3. KINETIC INDUCTANCE MODELLING

Given a metal strip with a rectangular cross section, having physical dimensions of length L , width W and thickness T , the associated geometrical resistance R_{G_0} and inductance L_{G_0} for this uniform strip are given by:

$$R_{G_0} = \frac{1}{\sigma_0} \left(\frac{L}{WT} \right) [\Omega] \quad \text{and} \quad L_{G_0} = \frac{1}{\omega\sigma_0} \left(\frac{L}{WT} \right) \propto (\omega\tau)^{-1} [\text{H}] \quad (11)$$

With the classical skin-effect model, at high frequencies such that the thickness dimension corresponds to a uniform current distribution given by the normal skin depth δ_{So} , these become:

$$R_{Go} \equiv R_{So} \left(\frac{L}{W} \right) \quad \text{when } T \rightarrow \delta_{So}$$

$$\text{where } R_{So} = \frac{1}{\sigma_o \delta_{So}} \quad [\Omega/\text{square}] \quad (12)$$

$$L_{Go} \equiv L_{So} \left(\frac{L}{W} \right) \quad \text{when } T \rightarrow \delta_{So}$$

$$\text{where } L_{So} = \frac{1}{\omega \sigma_o \delta_{So}} = \frac{X_{So}}{\omega} \quad [\text{H}/\text{square}] \quad (13)$$

The geometrical inductance L_{Go} , corresponds to the internal magnetic inductance associated with the energy stored in the external magnetic field. However, with the classical relaxation-effect model, it will be seen that in addition to L_{Go} , kinetic inductance is created from the inertial mass of a mobile charge carrier distribution within an alternating electric field. This additional inductance is normally associated with superconductors [9, 10]; however, as will be seen here, it can also serve to give a useful pedagogical insight into how the classical skin-effect and relaxation-effect models differ, within a normal metal at room temperature, as well as providing a useful variable for simplifying analytical expressions.

The force F exerted by an electric field having an intensity E on an electron with charge e is given by $\hat{F} = e\hat{E}$. Therefore, the time-average momentum of the inertial mass of an electron within a uniform dc electric field, $\langle \hat{p} \rangle = \int_0^\tau \hat{F}(t) dt = e\tau \hat{E}$. Also, $\langle \hat{p} \rangle = m\langle \hat{v}_d \rangle$, where m is the mass of the electron and $\langle \hat{v}_d \rangle$ is the time-average drift velocity for the inertial mass of an electron. The conduction current density is $\hat{J}_c = Ne \langle \hat{v}_d \rangle$ [A/m²], where N is the volume density of free electrons. Therefore, the well-known expression for the dc case gives $\hat{J}_c = (Ne^2\tau/m) \hat{E} \equiv \sigma_o \hat{E}$ and so $\sigma_o = (Ne^2\tau/m) \propto \tau$.

A mobile charge carrier distribution will have an inertial mass that tries to oppose any change in electromotive force. The kinetic energy stored by the inertial mass of this electron distribution can be equated to that stored by a magnetic field and, therefore, represented by an equivalent geometrical kinetic inductance L_{Gk} for the metal strip. The kinetic energy density E_{Dk} is given by $E_{Dk} = 0.5(Nm)\langle v_d \rangle^2$ [J/m³]. Therefore, the kinetic energy, $E_k = E_{Dk}(LWT \equiv 0.5 L_{Gk} I^2$, where the transport current is given by $\hat{I} = Ne\langle \hat{v}_d \rangle(WT)$. As a result, the

following expression for L_{Gk} can be extracted:

$$L_{Gk} = \left(\frac{m}{Ne^2} \right) \left(\frac{L}{WT} \right) \equiv \frac{\tau}{\sigma_o} \left(\frac{L}{WT} \right) \neq f(\omega\tau) \quad [\text{H}] \quad (14)$$

From (11) and (14), it can now be seen that the geometrical kinetic inductance is directly proportional to the geometrical inductance for the uniform metal strip, with the constant of proportionality given by $(\omega\tau)$; a term which is directly proportional to the frequency of the driving electromagnetic fields and inversely proportional to physical temperature.

$$\therefore L_{Gk} \equiv (\omega\tau) L_{Go} \quad (15)$$

$$L_{Gk} \equiv L_k \left(\frac{L}{W} \right) \text{ when } T \rightarrow \delta_o$$

$$\text{where } L_k = \frac{\tau}{\sigma_o \delta_{So}} = \tau R_{So} \text{ [H/square]} \quad (16)$$

Here, the kinetic surface inductance L_k is also directly proportional to the surface inductance from the classical skin-effect model, with the constant of proportionality given by $(\omega\tau)$:

$$\therefore L_k \equiv (\omega\tau) L_{So} \quad (17)$$

It can be easily shown, using (17) with (6) and (8), that both shunt elements within the elementary lumped-element circuit of Fig. 3(b) are related to the kinetic series inductance, as given in (18):

$$G_R \equiv \frac{\sigma_o}{\left[1 + \left(\frac{L_k}{L_{So}} \right)^2 \right]} \quad \text{and} \quad L_{SHUNT_R} \equiv \text{constant} \cdot \left[1 + \left(\frac{L_{So}}{L_k} \right)^2 \right] \quad (18)$$

It is interesting to note that, with the classical relaxation-effect model, the imaginary part of bulk conductivity is also directly proportional to its real part, with the constant of proportionality given by $(\omega\tau)$, and, therefore, also related to the kinetic series inductance:

$$\sigma''_R = (\omega\tau) \sigma'_R \text{ and } \sigma''_R = \left(\frac{L_k}{L_{So}} \right) \sigma'_R \quad (19)$$

It can be clearly deduced that C_R , L_{SHUNT_R} , L_{Gk} , L_k and σ''_R are all insignificant when $\omega\tau \ll 1$, i.e., as found with the classical skin-effect model.

Now, for the classical relaxation-effect model, the surface impedance Z_{SR} is given by the following [6]:

$$Z_{SR} = Z_{So} \sqrt{1 + j\omega\tau} = R_{So} \left(x + j \frac{1}{x} \right) \quad (20)$$

$$x = \sqrt{\sqrt{1 + u^2} - u}; \quad \frac{1}{x} = \sqrt{\sqrt{1 + u^2} + u}$$

From (6), it can be seen that:

$$Z_{SR} = R_{So} \left[\frac{1}{(1 + \xi \omega \tau)} + j(1 + \xi \omega \tau) \right] \tag{21}$$

$$X_{SR} = X_{So} + \xi X_k = \omega L_{SR} \quad \text{where} \quad X_k = \omega L_k$$

Therefore, from (13) and (21), with the classical relaxation-effect model, the surface inductance L_{SR} can be given by the following expression:

$$L_{SR} = L_{So} + \xi L_k = L_{So} (1 + \xi \omega \tau)$$

$$L_{So} = \mu \left(\frac{\delta_{So}}{2} \right) \propto (\omega \tau)^{-1/2} \quad \text{and} \quad L_k = \frac{\tau}{\sigma_o \delta_{So}} \propto (\omega \tau)^{+1/2} \tag{22}$$

In terms of kinetic inductance, it can also be shown that:

$$R_{SR} = \frac{L_{So}}{(L_{So} + \xi L_k)} \left(\frac{L_k}{\tau} \right) \quad \text{and} \quad X_{SR} = \left(1 + \xi \frac{L_k}{L_{So}} \right) \left(\frac{L_k}{\tau} \right) \tag{23}$$

Frequency plots of surface reactance for both the classical skin-effect and relaxation-effect models are shown in Fig. 6(a) for gold at room temperature. The contribution to the latter from the kinetic surface inductance is also given. Of major significance, in terms of further simplifying analytical expressions, it has been found that the variable $\xi = f(\omega \tau)$, given by (7), is equal to a constant value

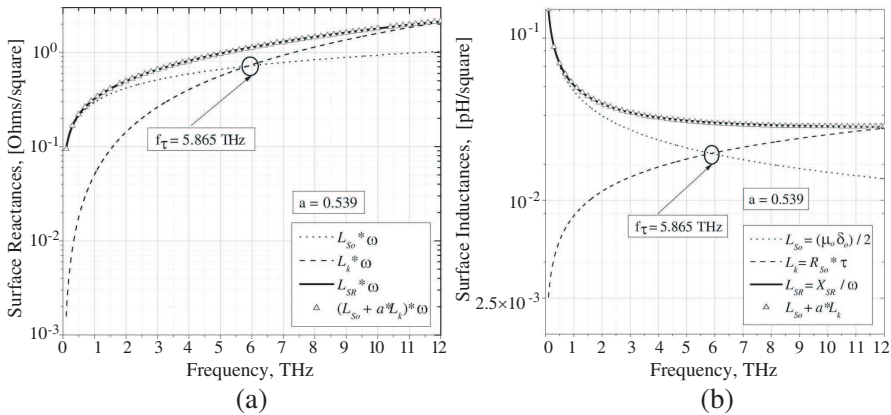


Figure 6. Calculated values for gold at room temperature: (a) surface reactance X_s and (b) corresponding surface inductance $L_s = X_s/\omega$.

$a = (\sqrt{1 + \sqrt{2}} - 1)$ at $\omega\tau = 1$. This constant value of a will give zero error at $\omega\tau = 1$ for the calculated values of surface inductance and reactance, but these errors increase to 2.39% as $\omega\tau$ increases to 2. However, it has been found empirically that a constant value of $a = 0.539$ will result in a worst-case error of only 0.96% from dc to $\omega\tau = 2$. The result of this approximation is also shown in Fig. 6. It can be seen that there is an excellent fit between the results using this approximation and the exact solution using ξ , for the classical relaxation-effect model for $0 \leq \omega\tau \leq 2$. Fig. 6(b) shows all the corresponding plots for the equivalent surface inductance, given in (22). Here, the surface inductance associated with energy stored in the actual external magnetic field decreases as a function of $(\omega\tau)^{-0.5}$; while that associated with kinetic energy stored by the inertial mass of the electron distribution increases as a function of $(\omega\tau)^{+0.5}$. Indeed, the kinetic surface inductance will dominate the classical skin-effect surface inductance above $\omega\tau = 1$, i.e., at $f_r = 1/(2\pi\tau) = 5.865$ THz shown in Fig. 6, and therefore kinetic inductance cannot be ignored at terahertz frequencies.

4. Q-FACTOR MODELLING

As its name suggests, the electrical quality (or Q)-factor usually represents a useful figure-of-merit by which materials, components or circuits can be compared in terms of their power loss. This section adopts this concept for analytical purposes. It has been found that the Q -factor represents a useful variable for the simplification of algebraic expressions associated with the mathematical modelling of intrinsic frequency dispersion within normal metals at room temperature.

4.1. Material Q -factor

Defining the Q -factor for a material Q_m is usually reserved for a dielectric or semiconductor, and represented by the following expression:

$$Q_m = \frac{1}{\tan \delta} = \left| \frac{\Re \{ \varepsilon_r \text{ effective} \}}{\Im \{ \varepsilon_r \text{ effective} \}} \right| \quad (24)$$

However, the same concept can be applied to normal metals at room temperature. Given the following general material relationships for equivalent conductivity $\sigma_{equivalent} = (\sigma + j\omega\varepsilon) \equiv j\omega\varepsilon_0\varepsilon_r \text{ equivalent}$, refractive index $n = \sqrt{\mu_r\varepsilon_r \text{ equivalent}} \equiv n' - jn''$, surface impedance $Z_S = \sqrt{j\omega\mu/\sigma_{equivalent}} = \eta_0\mu_r/n$ and propagation constant $\gamma = j\omega\mu/Z_S = \sqrt{j\omega\mu\sigma_{equivalent}} = j\omega\sqrt{\mu\varepsilon_0\varepsilon_r \text{ equivalent}} = \gamma_0 n$, (where,

$\eta_o = \sqrt{\mu_o/\varepsilon_o}$ and $\gamma_o = j\omega\sqrt{\mu_o\varepsilon_o}$ are the intrinsic impedance and propagation constant, respectively, for a plane wave in free space), it can be seen that the following represent equally valid definitions for the Q -factor of a normal metal at room temperature:

$$Q_m = \frac{\Re\{n^2\}}{\Im\{n^2\}} = \frac{\Re\{\gamma^2\}}{\Im\{\gamma^2\}} = \frac{\Im\{\sigma_{equivalent}\}}{\Re\{\sigma_{equivalent}\}} = \frac{-\Re\{Z_S^2\}}{\Im\{Z_S^2\}}$$

$$\Rightarrow \begin{cases} \equiv 0 & \text{for } Q_{mo} \\ > 0 & \text{for } Q_{mR} \end{cases} \quad (25)$$

4.2. Component Q -factor

Defining the unloaded Q -factor for an electrical component Q_c is usually reserved for a physical passive device or resonant circuit (given a reactance X_c and equivalent series loss resistance R_c or alternatively a susceptance B_c and equivalent parallel loss conductance G_c) and represented by the following:

$$Q_c = \frac{|X_c|}{R_c} = \frac{|B_c|}{G_c} \quad (26)$$

However, again, the same concept can be applied to normal metals at room temperature, since its surface impedance has both resistive and reactive parts:

$$Q_c = \frac{\Im\{n\}}{\Re\{n\}} = \frac{\Re\{\gamma\}}{\Im\{\gamma\}} = \frac{\Im\{Z_S\}}{\Re\{Z_S\}} \Rightarrow \begin{cases} \equiv 1 & \text{for } Q_{co} \\ > 1 & \text{for } Q_{cR} \end{cases} \quad (27)$$

For a normal metal, Q_m and Q_c are interrelated by the following expressions:

$$Q_m = \left| \frac{1 - Q_c^2}{2Q_c} \right| \quad \text{and} \quad Q_c = Q_m + \sqrt{1 + Q_m^2} \quad (28)$$

For the classical relaxation-effect model, it can be shown that:

$$Q_{mR} \equiv (\omega\tau) \quad \text{and} \quad Q_{cR} \equiv \frac{1}{x^2} = (1 + \xi Q_{mR})^2 \quad (29)$$

Both material and component Q -factors are plotted in Fig. 7 for gold at room temperature, where it can be seen that for the classical relaxation-effect model they simplify greatly to $Q_{mR} = 1$ and $Q_{cR} = (1 + \sqrt{2})$, respectively, at $\omega\tau = 1$ and also $Q_{cR} \approx 2Q_{mR} = 2(\omega\tau)$ when $\omega\tau \gg 1$. It is interesting to note that, with the former relationship for Q_{cR} , when given the measured optical constants against either frequency, wavelength, wavenumber or energy, $\omega\tau = 1$ can be determined when $n''/n' = (1 + \sqrt{2})$.

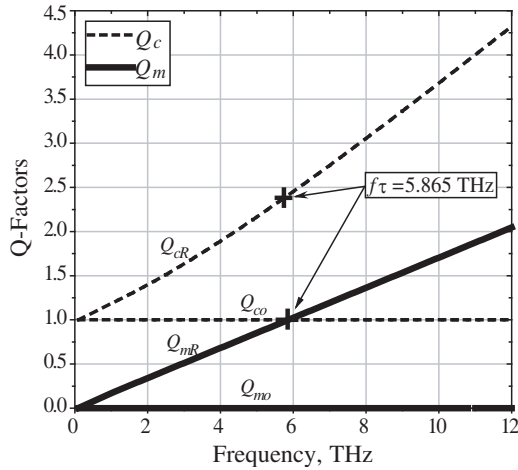


Figure 7. Calculated values of material (solid line) and component (dotted line) Q -factors with the classical relaxation-effect model for gold at room temperature.

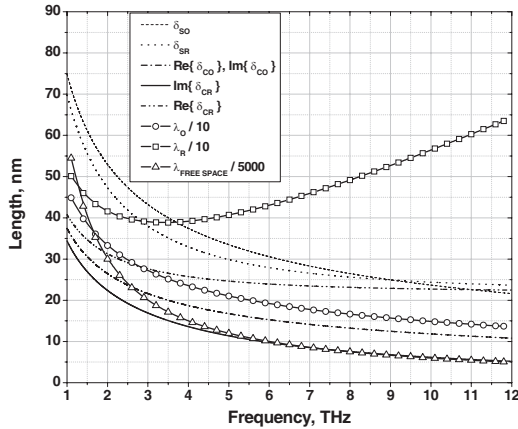


Figure 8. Calculated values of various skin depths and wavelengths for gold at room temperature.

In terms of surface inductances, it can also be shown that:

$$Q_{mR} \equiv \left(\frac{L_k}{L_{So}} \right) \text{ and } Q_{cR} \equiv \left(\frac{L_{SR}}{L_{So}} \right)^2 \quad (30)$$

It will be seen that these Q -factor terms can be very useful for simplifying analytical expressions. For example, using (29), the

expression for surface impedance in (21) can be greatly simplified to the following:

$$Z_{SR} = R_{So} \left(\frac{1}{\sqrt{Q_{cR}}} + j\sqrt{Q_{cR}} \right) = R_{SR} (1 + jQ_{cR}) \quad (31)$$

Also, the propagation constant per unit wavelength of the electromagnetic fields as they try to propagate into a normal metal at room temperature is given by the following:

$$e^{-\gamma_R \lambda_R} = e^{-2\pi \gamma_R / \Im\{\gamma_R\}} = e^{-2\pi(Q_{cR} + j)} \rightarrow e^{-2\pi(1 + \sqrt{2})} [Np/\lambda_R] \quad \text{at } \omega\tau = 1 \quad (32)$$

As another example, with both distributed-element models in Fig. 3, since $\Delta z \ll \lambda_R$, the unloaded component Q -factor for a single elementary lumped-element circuit can be shown to be equal to the material Q -factor as follows:

$$Q_{cR} (\Delta z \ll \lambda_R) \Rightarrow \frac{|\omega C_R|}{G_R} = \frac{1}{(G_R \Delta z) (\omega L_{SHUNT_R} \Delta z)} = (\omega\tau) \equiv Q_{mR} \quad (33)$$

5. MODELLING WITH COMPLEX SKIN DEPTH

For the electromagnetic wave, as it tries to propagate into a normal metal at room temperature, the relationship between propagation constant γ , normal skin depth δ_S , wavelength λ and complex skin depth δ_c are shown below:

$$\begin{aligned} \gamma &\equiv \alpha \text{ [Np/m]} + j\beta \text{ [radians/m]} \\ \delta_S &= \frac{1}{\alpha} \text{ [m]} \quad \text{and} \quad \lambda = \frac{2\pi}{\beta} \text{ [m]} \quad \text{and} \quad \delta_c = \frac{1}{\gamma} \equiv \delta'_c - j\delta''_c \text{ [m]} \end{aligned} \quad (34)$$

where α and β are the attenuation and phase constants, respectively. For the classical skin-effect model, these become:

$$\begin{aligned} \gamma_o &\equiv \beta_o(1 + j) \quad \text{where} \quad \alpha_o = \beta_o \\ \delta_{So} &= \frac{1}{\alpha_o} \quad \text{and} \quad \lambda_o = \frac{2\pi}{\beta_o} = 2\pi\delta_{So} \quad \text{and} \quad \delta_{co} = \frac{1}{\gamma_o} = \frac{\delta_{So}}{2} (1 - j) \end{aligned} \quad (35)$$

At low frequencies, normal skin depth for the classical skin-effect model $\delta_{So} = 1/(\sigma_o R_{So})$ is widely quoted in both textbooks and research papers. For the classical relaxation-effect model the relationships

become:

$$\begin{aligned} \gamma_R &\equiv \beta_R(Q_{cR} + j) \quad \text{where} \quad \alpha_R = \beta_R Q_{cR} \\ \delta_{SR} &= \frac{1}{\alpha_R} = \Re\{\delta_{cR}\} \left(1 + \frac{1}{Q_{cR}^2}\right) \quad \text{and} \quad \lambda_R = \frac{2\pi}{\beta_R} = 2\pi\delta_{SR} \cdot Q_{cR} \quad (36) \\ \delta_{cR} &= \frac{1}{\gamma_R} = \Re\{\delta_{co}\} \left(\sqrt{Q_{cR}} - j\frac{1}{\sqrt{Q_{cR}}}\right) = \Im\{\delta_{cR}\} (Q_{cR} - j) \end{aligned}$$

The various skin depths and wavelengths for gold at room temperature are plotted in Fig. 8, for the two classical intrinsic frequency dispersion models. In addition, for comparison, the wavelength in free space has also been included; highlighting the fact that electromagnetic waves within gold at room temperature are effectively slowed down by a factor of approximately 500. It can be seen in Fig. 8 that, with the classical relaxation-effect model, the normal skin depth is less than that calculated with the classical skin-effect model, i.e., $\delta_{SR} < \delta_{So}$, below $\omega\tau = (1 - \xi)/\xi^2 \approx 1.587$ and $\delta_{SR} > \delta_{So}$ above this frequency. Also, $\Re\{\delta_{cR}\} = \delta_{So}$ at $\omega\tau = 1/\xi \approx 1.855$.

Apart from calculating the minimum acceptable thickness of shielding metal walls and guided-wave structures, complex skin depth is far more meaningful than the normal skin depth, because it takes the phase constant into account, as well as being a useful variable for simplifying analytical expressions.

One striking feature in Fig. 8 is that, well beyond its turning point at $\omega\tau = 1/\sqrt{3} \cong 0.5774$, the classical relaxation-effect model wavelength increases proportionally with frequency. This is counter intuitive but, nevertheless, mathematically correct because it can now be easily determined that this wavelength is given by the following expressions:

$$\begin{aligned} \lambda_R = 2\pi\Im\{\delta_{cR}\} (1 + Q_{cR}^2) = \frac{\lambda_o}{2} \left(\frac{1 + Q_{cR}^2}{\sqrt{Q_{cR}}}\right) \rightarrow \text{constant} \cdot \left(\frac{L_k}{L_{so}}\right) \propto \omega\tau \\ \text{when } \omega\tau \gg 1 \quad (37) \end{aligned}$$

Other examples of how exact analytical expressions can be greatly simplified using complex skin depth terms will now be given. For instance, the conduction current density $J_c(z)$ for a normal metal at room temperature decays exponentially with distance z into the metal, according to the complex exponent term $-z/\delta_c$, from its surface value $J_c(0)$ given by:

$$\hat{J}_c(0) [\text{A/m}^2] = \frac{\hat{J}_S [\text{A/m}]}{\delta_c [\text{m}]} \quad (38)$$

where J_S is the surface current density. As other examples, for the classical relaxation-effect model, the surface impedance, phase velocity,

surface inductance and component Q -factor can all be represented simply by using complex skin depth terms:

$$Z_{SR} = j\omega\mu\delta_{cR} = \omega\mu(\Im\{\delta_{cR}\} + j\Re\{\delta_{cR}\})$$

$$\text{and } v_{pR} = \frac{\omega}{\beta_R} = \omega \frac{|\delta_{cR}|^2}{\Im\{\delta_{cR}\}} \text{ [m/s]} \quad (39)$$

$$L_{SR} = \mu\Re\{\delta_{cR}\} \quad \text{and} \quad Q_{cR} = \frac{\Re\{\delta_{cR}\}}{\Im\{\delta_{cR}\}} = \left(\frac{\Re\{\delta_{cR}\}}{\Re\{\delta_{co}\}} \right)^2 \quad (40)$$

A more practical example can be found with the unloaded Q -factor for an air-filled metal-pipe rectangular waveguide cavity resonator. It can be shown that, for the special case of a half-height cavity resonator having equal internal width and length spatial dimensions, with non-magnetic (i.e., $\mu_r = 1$) normal metal walls at room temperature, the unloaded Q -factor Q_U for the dominant TE_{101} mode at its resonant frequency ω_{oR} can be represented by the following:

$$Q_{uR}(\omega_{oR})|_{TE_{101}} \cong \frac{\text{Internal Volume [m}^3]}{\text{Internal Surface Area [m}^2] \cdot \Im\{\delta_{cR}(\omega_{oR})\}[\text{m}]} \quad (41)$$

This expression is both intuitive and elegant. The more general form of (41), for the relaxation-effect model, was previously reported without any formal proof [6] and a full derivation has recently been given [7] using some of the tools outlined in this paper.

6. CONCLUSION

This paper has introduced various interrelated electrical engineering concepts as tools for characterizing the intrinsic frequency dispersive nature of normal metals at room temperature. This engineering approach dramatically simplifies otherwise complex analysis and allows for a much deeper insight to be gained into the classical relaxation-effect model. For example, it explains how wavelength can increase proportionally with frequency at higher terahertz frequencies. While relatively simple examples have been given here to show how algebraic expressions can be dramatically simplified, similar benefits can also be achieved with more complicated analytical problems [7].

This is the first time that such an approach has been developed for the modelling of intrinsic frequency dispersion within a metal. While the focus has been on the characterization of normal metals (magnetic and non-magnetic) at room temperature, it is believed that the same methodology may also be applied to metals operating in anomalous frequency-temperature regions, superconductors, semiconductors, carbon nanotubes and metamaterials.

ACKNOWLEDGMENT

This work was supported by the UK's Engineering and Physical Sciences Research Council (EPSRC) under Platform Grant EP/E063500/1.

REFERENCES

1. Drude, P., "Zur elektronentheorie der metalle," *Annalen Der Physik*, Vol. 306, No. 3, 566–613, 1900.
2. Drude, P., "Zur elektronentheorie der metalle; II. Teil. galvanomagnetische und thermomagnetische effecte," *Annalen Der Physik*, Vol. 308, No. 11, 369–402, 1900.
3. Lucyszyn, S., "Investigation of anomalous room temperature conduction losses in normal metals at terahertz frequencies," *IEE Proceedings — Microwaves, Antennas and Propagation*, Vol. 151, No. 4, 321–329, 2004.
4. Lucyszyn, S., "Investigation of Wang's model for room temperature conduction losses in normal metals at terahertz frequencies," *IEEE Trans. on Microwave Theory Tech.*, Vol. 53, 1398–1403, 2005.
5. Lucyszyn, S., "Evaluating surface impedance models for terahertz frequencies at room temperature," *PIERS Online*, Vol. 3, No. 4, 554–559, 2007.
6. Zhou, Y. and S. Lucyszyn, "HFSSTM modelling anomalies with THz metal-pipe rectangular waveguide structures at room temperature," *PIERS Online*, Vol. 5, No. 3, 201–211, 2009.
7. Lucyszyn, S. and Y. Zhou, "THz applications for the engineering approach to modelling frequency dispersion within normal metals at room temperature," *PIERS Online*, Vol. 6, No. 3, 293–299, Feb. 2010.
8. Kraus, J. D., *Electromagnetics*, 4th edition, 587–588, McGraw-Hill, 1991.
9. Pond, J. M., J. H. Claassen, and W. L. Carter, "Kinetic inductance microstrip delay lines," *IEEE Transactions on Magnetism*, Vol. 23, No. 2, 903–906, 1987.
10. McDonald, D. G., "Novel superconducting thermometer for bolometric applications," *Appl. Phys. Lett.*, Vol. 50, No. 12, 775–777, 1987.